16. Y. K. Agrawal, D. W. Short, R. Gruenke, and R. A. Rapp, *ibid.*, **121**, 354 (1974).
17. H. R. Thirsk and J. A. Harrison, "A Guide to the Study of Electrode Kinetics," Academic Press, London and New York (1972).
18. F. P. Netzer and H. L. Gruber, *Z. Phys. Chem. N.F.*, **85**, 159 (1973).
19. R. Lewis and R. Gomer, *Surf. Sci.*, **12**, 157 (1968).
20. T. M. Gür, I. D. Raistrick, and R. A. Huggins, *This Journal*, **127**, 2620 (1980).
21. D. Brennan, D. O. Hayward, and B. M. W. Trapwell, *Proc. R. Soc. London, Ser. A*, **256**, 81 (1960).

Oxygen Transfer on Substituted ZrO_2, Bi_2O_3, and CeO_2 Electrolytes with Platinum Electrodes

II. A-C Impedance Study

M. J. Verkerk[1] and A. J. Burggraaf

Twente University of Technology, Department of Chemical Engineering, Laboratory of Inorganic Chemistry and Materials Science, 7500 AE Enschede, The Netherlands

ABSTRACT

An equivalent electrical circuit that describes the electrode processes on different electrolytes, using porous Pt electrodes, is given. Diffusional processes are important and have to be presented by Warburg components in the circuit. The overall electrode process is rate limited by diffusion of atomic oxygen on the electrode surface for stabilized zirconia and substituted ceria (low P_{O_2}). On stabilized bismuth sesquioxide diffusion of atomic oxygen on the electrolyte surface is rate limiting at high P_{O_2} while at low P_{O_2} another process, probably diffusion of electronic species in the electrolyte, is dominant. One of these processes plays a role too on substituted ceria at high P_{O_2}, where a charge transfer process is dominant. These results are consistent with the mechanisms developed in part I of this paper.

In part I of this paper (1) a d-c study was performed on solid electrolytes based on ZrO_2, CeO_2, and Bi_2O_3 with platinum electrodes. It was concluded that for ZrO_2- and CeO_2-based materials the oxygen atoms for the electrode process are mainly supplied by dissociative adsorption of oxygen molecules at the Pt electrode, followed by transport to the reaction site where the charge transfer occurs. For Bi_2O_3-based materials the dominant adsorption and diffusion steps (in the high P_{O_2} and low temperature region) take place on the electrolyte. This different adsorption behavior is the origin of the lower electrode resistance of a Pt electrode on Bi_2O_3-based materials in comparison with that on ZrO_2- and CeO_2-based materials. Frequency dispersion analysis is a powerful tool for studying in detail the mechanism of the electrode process on these electrolytes (2-4).

Various authors studied the frequency behavior of Pt electrodes on a solid electrolyte. Generally, for Pt-paste and Pt-sputtered electrodes on stabilized zirconia the part of the frequency dispersion diagram which corresponds to the electrode process consists of a depressed semicircle (2, 5-9). This is interpreted in terms of a parallel combination of a resistance and a double layer capacity (2). A Warburg-type behavior, which is characteristic for diffusion limitation, is sometimes observed at high temperatures and low oxygen partial pressures (5, 8, 10). For Pt-paste electrodes on substituted ceria Braunshtein *et al.* (11) found that the overall process consists of a parallel combination of a resistance and a Warburg impedance. However, Wang and Nowick (12) observed for a Pt-paste electrode on substituted ceria a depressed semicircle, which interpretation is not very clear. The electrode process on (porous) Bi_2O_3 was studied using Au-paste electrodes (13, 14). The experimental results are interpreted in terms of a parallel combination of a resistance and Warburg impedances. The Warburg impedances are correlated with diffusion on the oxide surface and on the metal surface (14). These data can hardly be used for obtaining insight on the influence of the electrolyte on the electrode process because the measurements were performed under different experimental conditions and using different electrode morphologies, which are sometimes badly characterized.

The object of this paper is to study in detail the mechanism of the electrode process on different electrolytes using frequency dispersion analysis and to support the models of the electrode process developed in part I of this study. With the frequency dispersion technique an equivalent electrical circuit of the electrode process can be achieved and resolved in its components and a further insight in the influence of the electrolyte on the electrode process can be obtained.

The following systems were studied:

$(ZrO_2)_{0.83}(YO_{1.5})_{0.17}$ (ZY17),

$(CeO_2)_{0.90}(GdO_{1.5})_{0.10}$ (CG10),

$(Bi_2O_3)_{1-x}(Er_2O_3)_x$ with $x = 0.20$, 0.30, and 0.40 (BE20, BE30, and BE40). Electrodes with the same morphology were realized on these electrolytes and this morphology was preserved during the subsequent experiments. The electrode preparation and characterization is thoroughly described in part I of this study. Experimental details concerning the preparation and characterization of electrolytes and the electrical measurements are given in Ref. (1). The procedure to determine the individual components of the equivalent electrical circuit is described elsewhere (27).

Theory

In part I of this study it was concluded that the rate-limiting step in the electrode process on ZY17, CG10 ($P_{O_2} < P_{O_2}^{min.}$), BE20, BE30, and BE40 is mass transport of oxygen atoms. In this section the relevant theory for the frequency dispersion behavior of a mass transport controlled reaction is given.

When a d-c current passes through the electrolyte the oxygen atoms for the electrode process are supplied or removed by diffusion of oxygen atoms on the electrode surface and/or electrolyte surface. The oxygen atoms diffuse over a characteristic length δ from $x = \delta$ to the triple line at $x = 0$, where the charge transfer

[1] Present address: Philips Research Laboratories, Eindhoven, The Netherlands.

Key words: electrode resistance, solid electrolytes, oxygen transfer mechanism, complex impedance.

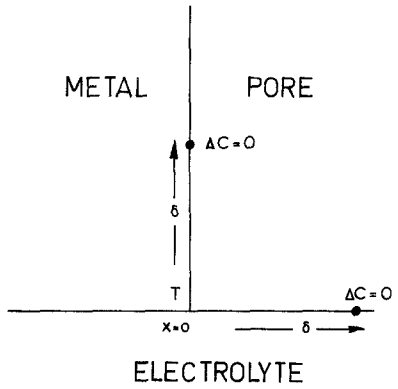

Fig. 1. Schematic picture of the diffusion process of oxygen atoms from $x = \delta$ to triple line T at $x = 0$.

takes place. The situation is depicted in Fig. 1. At $x \geqq \delta$ the concentration of adsorbed oxygen atoms is constant. The production or removal of oxygen atoms is so small that the equilibrium concentration at $x \geqq \delta$ is not changed during the experiments or for $x \geqq \delta$ the exchange of oxygen molecules with the gas phase is large enough to keep the concentration of oxygen atoms at $x \geqq \delta$ constant. It is assumed that across the distance δ the exchange of oxygen molecules with the gas phase has an ignorable effect on the concentration distribution in this area (δ is small in comparison with the size of the electrode particles).

In the case that an a-c current passes the electrolyte the "penetration depth" λ of the concentration perturbation, due to the production or removal of oxygen atoms at the triple line, is given by $\sqrt{2D_o/\omega}$, where D_o is the diffusion coefficient of oxygen atoms and ω is the frequency $\omega = 2\pi f$. For $\lambda < \delta$ the diffusion process occurs in a semi-infinite medium. For small frequencies the penetration depth will be limited by $\lambda_{max} = \delta$. The calculation of the impedance of this diffusion process for a comparable situation is given by Broers (15) for an electrode in aqueous solutions and molten salts and is summarized below.

The one-dimensional diffusion equation is given by

$$\frac{\partial \Delta C}{\partial t} = D_o \frac{\partial^2 \Delta C}{\partial x^2} \qquad [1]$$

where $\Delta C = C(x,t) - C_o$ and C_o is the equilibrium concentration. The boundary conditions are given by

$$x = \delta \quad \Delta C = 0 \qquad [2]$$

$$x = 0 \quad D_o \left(\frac{\partial \Delta C}{\partial x} \right)_{x=0} = \frac{i}{n\mathbf{F}} \qquad [3]$$

where n is the number of electrons involved in the electrode process. Assuming Nernst reversibility, the solution of the diffusion Eq. [1] using the boundary conditions [2] and [3] and the additional condition $|\Delta C| << C_o$ (which implies small overvoltages), is given by (14, 15)

$$Z_w = \frac{RT\delta}{n^2\mathbf{F}^2 C_o D_o} \times \frac{\tanh\,[\beta(1+j)]}{\beta(1+j)} \qquad [4]$$

where

$$\beta = \delta \sqrt{\frac{\omega}{2D_o}} \qquad [5]$$

A graphical representation of [4] is given in Fig. 2a and the admittance diagram correlated with this process is given in Fig. 2b.

If $\beta \geqq 3$, *i.e.*, the penetration depth λ is small with respect to the length δ, the diffusion occurs in an effectively semi-infinite medium and Eq. [4] is reduced to a classical Warburg impedance

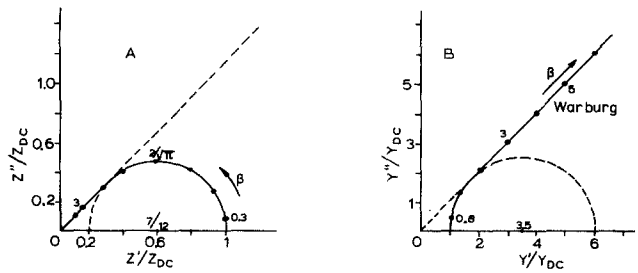

Fig. 2. Normalized impedance (A) and admittance (B) plots of the R-type Warburg impedance (Eq. [4]). [After (14, 15).]

$$Z_w = K_w \omega^{-1/2} \times (1 - j) \qquad [6]$$

where

$$K_w = \frac{RT}{n^2\mathbf{F}^2 C_o \sqrt{2D_o}} \qquad [7]$$

K_w is called the Warburg constant.

On the other hand, if $\beta \leqq 0.3$, *i.e.*, the penetration depth is limited by $x = \delta$, where $\Delta C = 0$, we find from [4]

$$Z_w = \frac{RT\delta}{n^2\mathbf{F}^2 C_o D_o} \qquad [8]$$

$$Z''/\omega = \frac{3RT}{n^2\mathbf{F}^2 C_o \delta} = \frac{1}{C_{LF}} \qquad [9]$$

where C_{LF} is the low frequency capacity.

For the maximum value of the imaginary component of [4] $\beta = 2/\sqrt{\pi}$ (see Fig. 2a). Using Eq. [5] the magnitude of $\delta/\sqrt{D}$ can be calculated without knowledge of the electrode area and the value of C_o and we find

$$\beta = 2/\sqrt{\pi} = \delta \sqrt{\frac{\omega_{max}}{2D_o}} \qquad [10]$$

where ω_{max} is the value of the frequency at the maximum value of the imaginary component of [4].

At low frequencies this type of Warburg behavior is like a resistance and is called "*R*-type Warburg impedance" (14).

Pt Electrodes on ZY17

Pt-sputtered electrodes.—In part I it was shown that in the relation between the electrode resistance R_{el} and the oxygen partial pressure a minimum in R_{el} appears at $P_{O_2} = P_{O_2}^{min.}$. Above and below $P_{O_2}^{min.}$ the electrochemical characteristics of R_{el} are quite different. At 983 K $P_{O_2}^{min.}$ has a value of about 4.5×10^{-2} atm O_2.

Figure 3 shows the complex impedance diagram at 983 K of sputtered electrodes on ZY17 as a function of the oxygen partial pressure. At $P_{O_2} > P_{O_2}^{min.}$ a single semicircle is observed (Fig. 3a). For $P_{O_2} \approx P_{O_2}^{min.}$ two overlapping semicircles are observed (Fig. 3b and c), indicating that two processes (connected in series) play a role. For $P_{O_2} < P_{O_2}^{min.}$ (Fig. 3d) the frequency dispersion diagram is interpreted in terms of a distorted Warburg impedance. It is shown (27) that interpretation of Fig. 3d in terms of two strongly overlapping semicircles is not correct. The development of the frequency dispersion diagrams as a function of the oxygen partial pressure was quite reproducible (using porous sputtered electrodes). The total equivalent electrical circuit is given in Fig. 4a. W_a is connected with diffusion at the anode. Generally, for W_a the condition $\beta \leqq 0.3$ holds over the whole frequency range investigated and W_a is reduced to a resistance R_a (Eq. [8]). This is discussed below. R_a varies with $P_{O_2}^{+1/2} \cdot W_c$ is connected with diffusion at the cathode and Z_{W_c} ($\omega \to 0$) $\sim P_{O_2}^{-1/2}$. This is discussed in the following.

At $P_{O_2} > P_{O_2}^{min.}$ the resistance R_a is large in comparison with the resistance of the Warburg impedance

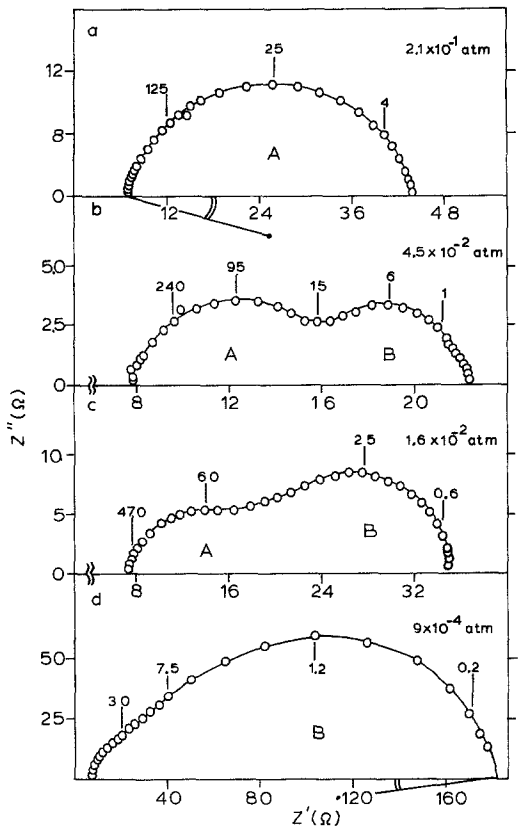

Fig. 3. The frequency dispersion diagrams of Pt-sputtered electrodes on ZY17 at 2.1 × 10^{-1} atm O_2 (a), 4.5 × 10^{-2} atm O_2 (b), 1.6 × 10^{-2} atm O_2 (c), and 9 × 10^{-4} atm O_2 (d). The temperature is 983 K. The frequency is given in Hz and is indicated by figures on the curves.

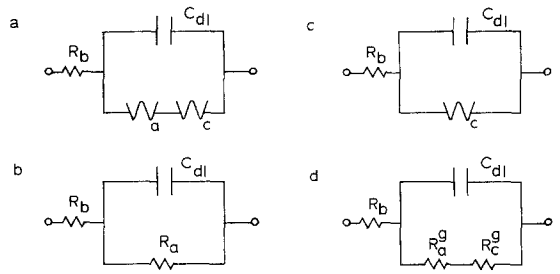

Fig. 4. Equivalent electrical circuits for Pt electrodes on ZY17. (a) Complete circuit for Pt-sputtered electrodes, (b) circuit for Pt-sputtered electrodes in the region of $P_{O_2} > P_{O_2}^{min.}$, (c) circuit for Pt-sputtered electrodes in the region of $P_{O_2} < P_{O_2}^{min.}$, (d) complete circuit for Pt-gauze electrodes. R_b, bulk resistance; C_{dl}, double layer capacity; W_a, Warburg impedance at the anode; W_c, Warburg impedance at the cathode; R_a, diffusion resistance at the anode (see text); R_a^g, diffusion resistance at the anode for gauze electrodes; R_c^g, diffusion resistance at the cathode for gauze electrodes.

W_c. Therefore in this region the equivalent circuit can be simplified to that shown in Fig. 4b and the frequency dispersion diagram is a semicircle, see Fig. 3a. The depression of the semicircle is independent of the oxygen partial pressure and the temperature and has a value of about 10°-20°. The capacity C_{dl} is independent of the oxygen partial pressure and the temperature (see Table I) and is therefore correlated with the double layer and has a value of about 2.8 F/m². From the frequency dispersion measurements it follows that $R_a \sim P_{O_2}{}^{+1/2}$ and $E_a(R_a)$ has a value of about 250 kJ mol^{-1}. This was already found in part I.

In part I of this study R_a was correlated with diffusion from the reaction site to the desorption site at $x = \delta$ (anodic process) and it was derived that $R_a \sim P_{O_2}{}^{+1/2}$ ($\theta \approx 1$). This result is supported by the experimental frequency dispersion diagram, which showed only resistive behavior in this case. The Warburg impedance given by Eq. [4] is reduced to a resistance if the condition $\beta \leq 0.3$ holds in the investigated frequency range. In our opinion this condition holds indeed at 983 K but not at lower temperatures. At 923 K in air the high frequency part of the frequency dispersion diagram deviates from a semicircle. The tangent of the high frequency part has an angle with the real axis of about 55° whereas the semicircle is depressed with 10°. This can be explained in the following way. At lower temperatures D_o is smaller and therefore the condition $\beta = \delta\sqrt{\omega/2D_o} \leq 0.3$ does only hold at low frequencies. At high frequencies this condition does not hold and the impedance of the diffusion process does not correspond with a simple resistance and the observed deviation appears.

At $P_{O_2} < P_{O_2}^{min.}$ the resistance R_a is small in comparison with the resistance of the Warburg impedance W_c. Therefore, in this region the equivalent circuit can be simplified to that shown in Fig. 4c and the experimental frequency dispersion diagram is shown in Fig. 3d. Figure 5 shows the complex impedance and admittance diagram at $P_{O_2} = 9 \times 10^{-4}$ atm O_2 after elimination of the bulk resistance and the double layer capacity from the circuit of Fig. 4c.

The diagrams shown in Fig. 5 have the same shape as those shown in Fig. 2a and b and are therefore correlated with a diffusion process. The experimentally found angle of the high frequency part of the diagrams with the real axis is 35°-37° instead of the theoretical value of 45°. The frequency dispersion diagram in $P_{O_2} = 1 \times 10^{-4}$ atm (not shown), after eliminating R_b and C_{dl}, has the same shape as that shown in Fig. 5. The values of C_{dl} and K_w are given in the Tables I and II, respectively.

Table I. Double layer capacity and low frequency capacity measured for the different electrode/electrolyte combinations

Material	Electrode	T (K)	Double layer capacity (F/m²)* 1.00 atm	0.60 atm	0.21 atm	0.10 atm	4.5 × 10^{-2} atm	1.6 × 10^{-2} atm	9 × 10^{-4} atm	10^{-4} atm
ZY17	Pt (sp)	1023			3.0					
		983	2.6	2.8	2.9	2.8	4.1	3.9	1.8	1.5
		923			3.9					
	Pt (g)	1023			10.9 × 10^{-2}					
		983	5.3 × 10^{-2}	6.8 × 10^{-2}	6.4 × 10^{-2}	9.2 × 10^{-2}	4.3 × 10^{-2}	7.3 × 10^{-2}	7.5 × 10^{-2}	7.4 × 10^{-2}
		923			5.5 × 10^{-2}					
CG10	Pt (sp)	983							0.8	1.0
BE30	Pt (sp)	973				10.4	11.4			33.8
BE40	Pt (sp)	973					14.6		10.4	7.0
			Low frequency capacity (F/m²)*							
ZY17	Pt (sp)	983					34	22	15	13

* The capacities are given per unit area of electrolyte and are not corrected for the size of the actual electrolyte/electrode contact surface. The values in this table are given for the two electrodes together.

Table II. Warburg constant for several systems as a function of the oxygen partial pressure

System	Temperature	Electrode	Kw (Ωm^2 $sec^{-1/2}$) 1 atm O_2	6×10^{-1} atm O_2	2.1×10^{-1} atm O_2	9×10^{-4} atm O_2	10^{-4} atm O_2
ZY17	983	sp				2.5×10^{-2}	3.5×10^{-2}
CG10	983	sp	1.2×10^{-2}	1.2×10^{-2}	1.4×10^{-2}	2.0×10^{-2}	2.3×10^{-2}
BE20	973	sp			4.9×10^{-4}		
	823	sp			9.5×10^{-4}		
BE40	973	sp			3.6×10^{-4}		
	823	sp			8.8×10^{-4}		

The low frequency resistance Z_{W_c} ($\omega \to 0$) varies with $P_{O_2}^{-1/2}$ and this agrees well with the results reported in part I, where it was concluded that the electrode resistance in this P_{O_2} region was correlated with diffusion of atomic oxygen from the adsorption site to the reaction site (cathodic process) and it was derived that the electrode resistance varies with $P_{O_2}^{-1/2}$ ($\theta << 1$).

For $P_{O_2} \approx P_{O_2}^{min.}$ both R_a and W_c play a role. At low frequencies the frequency dispersion diagram is determined by W_c whereas at high frequencies by R_a and C_{dl}, resulting in two overlapping semicircles.

The existence of two series connected processes, as given in the equivalent circuit in Fig. 4a, was not recognized before in literature (6, 9, 16).

Pt-gauze electrodes.—The complex impedance diagram for Pt-gauze electrodes on ZY17 consists of a depressed semicircle over the whole oxygen partial pressure range. The total equivalent electrical circuit is given in Fig. 4d with $R_a^g \sim P_{O_2}^{+1/2}$ and $R_c^g \sim P_{O_2}^{-1/2}$. For $P_{O_2} > P_{O_2}^{min.}$ the total electrode resistance is determined by R_a^g · R_a^g shows the same P_{O_2} dependence and the same value of E_a as R_a for sputtered electrodes and is therefore correlated with the same process, *i.e.*, diffusion limitation at the anode.

For $P_{O_2} < P_{O_2}^{min.}$ the total electrode resistance is determined by R_c^g. R_c^g has the same P_{O_2} dependence as Z_{W_c} ($\omega \to 0$) for sputtered electrodes and about the same value for the activation energy is found (see part I). Therefore, it is plausible that R_c^g represents the same process as W_c, *i.e.*, diffusion at the cathode. Due to the difference in electrode morphology between a sputtered and a gauze electrode the condition $\beta \leq 0.3$ holds for gauze electrodes (resulting in a depressed semicircle) to higher frequencies than for sputtered electrodes where a typical "Warburg-type behavior" is observed.

We conclude that the mechanism of the electrode reaction for gauze and sputtered electrodes is the same.

Diffusion path.—The diffusion paths correlated with W_a and W_c (R_a^g and R_c^g, respectively, for gauze electrodes) are now discussed. The processes W_a and W_c are correlated with an R-type Warburg impedance and therefore the condition $\Delta C = 0$ holds at $x = \delta$. This condition holds for the situation depicted in Fig. 1, where diffusion of atomic oxygen proceeds over a distance δ to the triple line. According to the preceding paper (part I) in the case of Pt electrodes on ZY17 the diffusion process should proceed on the Pt electrode.

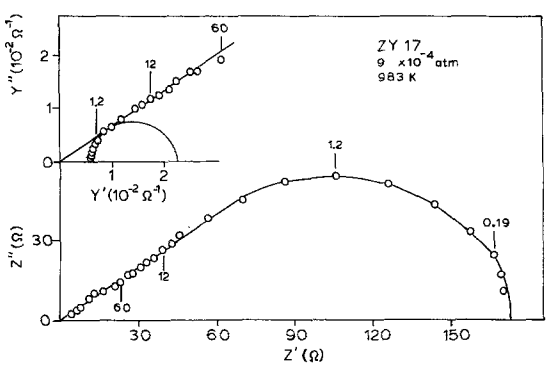

Fig. 5. Complex impedance diagram and complex admittance diagram for Pt-sputtered electrodes on ZY17 at $P_{O_2} = 9 \times 10^{-4}$ atm O_2 (983 K) after elimination of R_b and C_{dl}. The frequency is given in Hz.

The investigated frequency range, for the diffusion process underlying W_a, holds that $\beta \leq 0.3$. Using $\omega = 1000$, this condition is equivalent to $\delta/\sqrt{D_o} \leq 1.4 \times 10^{-2}$ $sec^{+1/2}$ (Eq. [5]). Lewis and Gomer (17) measured the surface diffusion of oxygen on (100)- and (111)-oriented Pt field emitters for $T > 500$ K and for low surface coverages. In the absence of better information we used these data to calculate D_o at 983 K and found a value of 1.2×10^{-11} m^2/sec. For the effective diffusion distance δ a value of ≤ 50 nm is calculated, which seems a reasonable value in view of the electrode morphology (particle size $\approx$ 1000 nm).

At $P_{O_2} < P_{O_2}^{min.}$ a value of $\delta/\sqrt{D_o}$ can be calculated according to Eq. [10] using ω_{max}. This value is estimated to be 0.58 and 1.16 $sec^{+1/2}$ at 9×10^{-4} and 10^{-4} atm O_2, respectively. Using the above-discussed value of $D_o = 1.2 \times 10^{-11}$ m^2/sec (19), δ is estimated to be 2 and 4 μm (at 9×10^{-4} and 10^{-4} atm O_2, respectively. These δ-values are too large taking into account the morphology of the electrode. Although there is a large uncertainty in the value of D_o, comparison of the δ-values at high P_{O_2} and at low P_{O_2} suggest that δ decreases with increasing P_{O_2} (18, 21).

According to Cahen (14) the condition $\Delta C = 0$ at $x = \delta$ holds also for a diffusion path between the two electrodes and the diffusion proceeds then on the oxide grains between the electrodes. This model can be applied for porous samples but is not very probable for our sample with a relative density of 99%. Furthermore, for our samples this diffusion process should proceed via the grain boundaries, whereas it was shown in part I that grain boundaries in pure ZY17 do not play a role in the electrode process. Braunstein *et al.* (11) concluded that a Warburg behavior should result from diffusion on the electrolyte/electrode interface (from the triple line). However, the current distribution assumed in their very simplified model is in contradiction with the distribution calculated on the basis of a physically more reasonable model (24). Furthermore, a recent analysis of Broers (23) showed that if the correct current distribution is taken into account, no Warburg behavior is found. Consequently, the electrolyte/electrode interface is not the dominant diffusion path.

Pt electrodes on CG10.—The frequency dispersion diagrams and the equivalent electrical circuit for Pt electrodes on CG10 are briefly discussed. The R_{el}-P_{O_2} relation for Pt electrodes on CG10 shows at 983 K a minimum in R_{el} for $P_{O_2} = 1.6 \sim 4.5 \times 10^{-2}$ atm O_2 (part I). For sputtered electrodes at $P_{O_2} > P_{O_2}^{min.}$ the frequency dispersion diagram consists of a quarter circle (comparable with Fig. 7a and b), at $P_{O_2} \approx P_{O_2}^{min.}$ of two overlapping semicircles (comparable with Fig. 3b and c) and at $P_{O_2} < P_{O_2}^{min.}$ of a distorted Warburg impedance (comparable with Fig. 3d). The total equivalent electrical circuit for sputtered electrodes is given in Fig. 6a. Experimentally R_{ct} is found to vary with $P_{O_2}^{+1/4}$ and Z_{W_c} ($\omega \to 0$) with $P_{O_2}^{-1/2}$. This is in a good agreement with the results of the d-c measurements, where R_{ct} was interpreted as a charge transfer resistance and Z_{W_c} ($\omega \to 0$) as a diffusion resistance at the

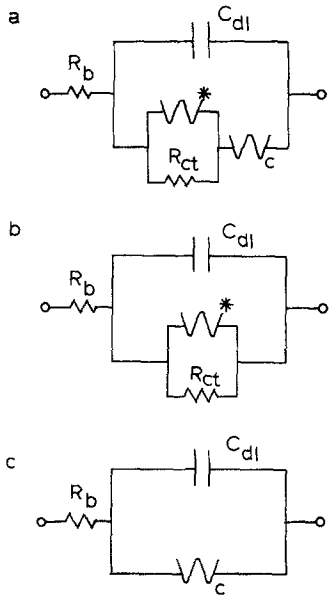

Fig. 6. Equivalent electrical circuit for Pt electrodes on CG10. (a) Complete circuit for Pt-sputtered electrodes, (b) circuit for Pt-sputtered electrodes in the region of $P_{O_2} > P_{O_2}^{min.}$, (c) circuit for Pt-sputtered electrodes in the region of $P_{O_2} < P_{O_2}^{min.}$, R_{ct}, charge transfer resistance; W^*, Warburg impedance. The meaning of the other symbols is given in the caption of Fig. 4.

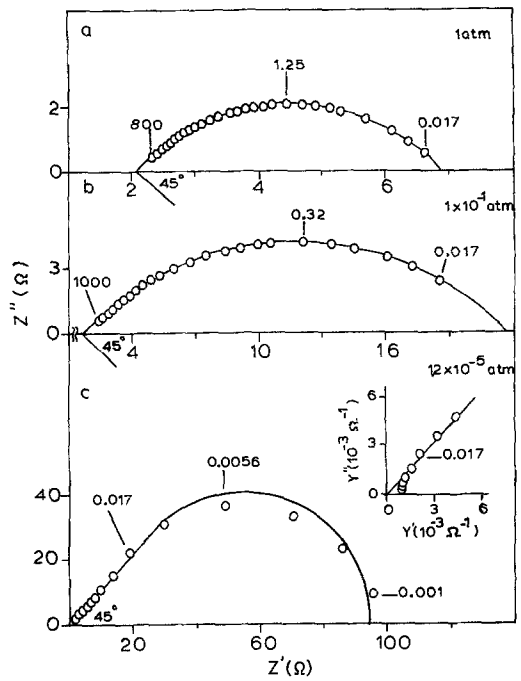

Fig. 7. Complex impedance diagrams for Pt-sputtered electrodes on BE20 at 1 atm O_2 (a), 1×10^{-1} atm O_2 (b), and 1.2×10^{-5} atm O_2 (c). The temperature is 973 K. In the impedance diagram shown in (c) the drawn line gives the theoretical plot for R-type Warburg behavior according to Eq. [4]. In (c) the admittance diagram is also given. The frequency is given in Hz.

cathode (part I). The equivalent circuit is now discussed.

At $P_{O_2} > P_{O_2}^{min.}$, R_{ct} is large in comparison with the impedance of W_c and the circuit is reduced to that shown in Fig. 6b; the impedance diagram consists of a quarter circle. (The influence of C_{dl} is only measurable at $P_{O_2} \leq P_{O_2}^{min.}$. W^* is semi-infinite over the frequency range measured and the K_w-value is given in Table II.

At $P_{O_2} \approx P_{O_2}^{min.}$ the frequency dispersion diagram is determined at low frequencies by W_c and at high frequencies by R_{ct}, W^*, and C_{dl} and this results in two overlapping semicircles.

At $P_{O_2} < P_{O_2}^{min.}$, R_{ct} is small compared with W_c and the circuit is reduced to that shown in Fig. 6c and results in a Warburg-type behavior. The values of K_{W_c} are summarized in Table II.

For Pt-gauze electrodes on CG10 the electrical equivalent circuit is also given by Fig. 6 and is discussed further elsewhere (25).

The P_{O_2} dependence and activation energy of Z_{W_c} ($\omega \to 0$) of Pt electrodes on CG10 is similar with that of Pt electrodes on ZY17. Furthermore for K_w the same value is found as on ZY17 (see Table II). Therefore we conclude that, similar to Pt electrodes on ZY17, W_c is correlated with diffusion on the Pt electrode.

At high P_{O_2} an additional Warburg impedance W^* was measured, which is parallel to R_{ct}. This impedance was not found for Pt electrodes on ZY17. This Warburg impedance W^* may be correlated with diffusion of atomic oxygen on the electrolyte or diffusion of electronic charge carriers through the electrolyte (which probably plays a role for Pt electrodes on stabilized Bi_2O_3, see below). More study is necessary to elucidate the origin of W^*.

Pt Electrodes on BE20, BE30, and BE40

Pt-sputtered electrodes.—Figure 7 shows the complex impedance behavior for Pt-sputtered electrodes on BE20 as a function of the oxygen partial pressure. The complete equivalent electrical circuit for sputtered electrodes on BE20, BE30, and BE40 is shown in Fig. 8a and is discussed. The double layer capacities were determined with the method described in Ref. (25) and its numerical values are summarized in Table I.

For BE20 the double layer capacity (in comparison with R and W) was too small to be measured. The double layer capacities measured for BE30 and BE40 are in good agreement with the values measured by Harwig (13) and Cahen (14) for gold-paste electrodes on pure Bi_2O_3 and are higher than found in this study for ZrO_2- and CeO_2-based materials. Consequently, the magnitude of C_{dl} is dominated by a process connected with the electrolyte.

At oxygen partial pressures in the range of $1\text{-}10^{-2}$ atm O_2 a perfect quarter circle is observed (Fig. 7a and b), representing a parallel combination of a resistance K and a Warburg impedance W. In the measured frequency range (10^3-10^{-2} Hz) the Warburg process is semi-infinite, *i.e.*, $\beta \geq 3$. Therefore, in this range the d-c resistance of the parallel R-W combination is determined by R because Z_w ($\omega \to 0$) is much larger than R. From the a-c study it follows that $R \sim P_{O_2}^{-1/2}$ and this is in a good agreement with the results of the d-c study (part I), where it was found additionally that $E_a(R) \approx 125$ kJ mol^{-1}.

At lower oxygen partial pressures ($< \omega^{-2}$ atm O_2) deviations appear at the low frequency part. These

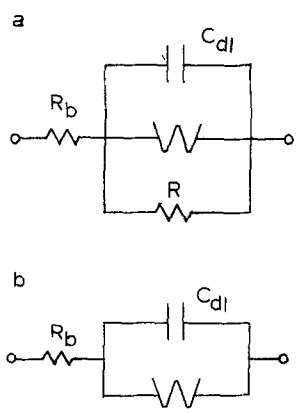

Fig. 8. (a) Complete equivalent electrical circuit for Pt electrodes on Bi_2O_3-based materials, (b) equivalent electrical circuit at low P_{O_2}. R, diffusion resistance; W, Warburg impedance. The meaning of the other symbols is given in the caption of Fig. 4.

deviations are due to the fact that under these circumstances the Warburg impedance is no longer semi-infinite. At $P_{O_2} = 1.2 \times 10^{-5}$ atm O_2 the electrode process is fully determined by the warburg impedance, as shown in Fig. 7c and the equivalent circuit is reduced to that shown in Fig. 8b. In this range the d-c resistance is determined by Z_w ($\omega \rightarrow 0$), which is characterized by an activation energy of about 50-90 kJ mol^{-1} (part I).

The value of the Warburg constant is not strongly dependent on the erbium concentration (27). K_w^{-1} varies with about $P_{O_2}^{1/4}$ and has an activation energy of about 35 kJ mol^{-1} (25).

Sputtered gold electrodes were not studied in detail. Frequency dispersion measurements showed that the equivalent electrical circuit is also given by Fig. 8a. At high oxygen partial pressures the impedance of the parallel R-W combination is determined by R. In part I it was shown that the E_a and P_{O_2} dependence of R for gold electrodes was the same as for platinum electrodes, which points to processes connected dominantly with the electrolyte.

These results support the conclusion of the preceding paper (part I) that R originates from diffusion of atomic oxygen on the oxide at the cathode [θ(oxide) $<< 1$].

Pt-gauze electrodes.—Figure 9a shows the complex impedance behavior for a Pt-gauze electrode on BE20 in oxygen and Fig. 9b shows the admittance behavior after eliminating the bulk resistance. The complete equivalent electrical circuit is given in Fig. 8a. The diagrams shown in Fig. 9 are representative of the diagrams in the oxygen partial pressure range of 1-10^{-5} atm O_2 and the shape is not influenced by the Er_2O_3 content.

The solid line in Fig. 9a gives the theoretical plot of the Warburg impedance. The deviation of the experimental data from this theoretical plot is caused by the resistance parallel to the Warburg impedance. The Warburg impedance is not semi-infinite and therefore the d-c resistance of the parallel R-W combination is determined by both R and W. As a consequence the experimentally found activation energy and P_{O_2} dependence is not characteristic for one process but is a combination of that belonging to R and W. Fitting procedures are necessary to separate the contribution of these components.

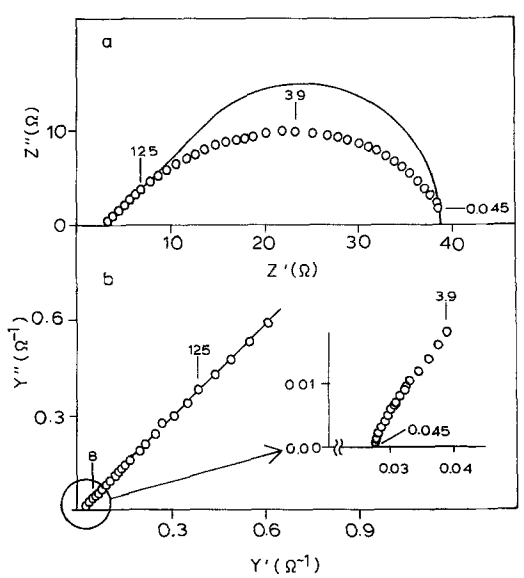

Fig. 9. (a) Complex impedance diagram for a Pt-gauze electrode on BE20 in oxygen at 1010 K. The solid line gives the theoretical plot for an R-type Warburg impedance after Eq. [4]. (b) Complex admittance plot after elimination of the bulk resistance. The frequency is given in Hz.

In our opinion, R varies with $P_{O_2}^{-1/2}$ and Z_w ($\omega \rightarrow 0$) varies with $P_{O_2}^{-1/4}$.[2] At high P_{O_2} the $-1/2$ power will dominate whereas at low P_{O_2} the $-1/4$ power will dominate. This interpretation is in a good agreement with the experimental data (see Fig. 7b from part I) and is confirmed by the good agreement of E_a(sp) and E_a(g) in the different regions (Table III, part I). This is also supported by the P_{O_2} dependence of K_w. For gauze electrodes we found that $K_w^{-1} \sim P_{O_2}^{1/4}$ (27). By comparing Eq. [7] and [8] we conclude that Z_w ($\omega \rightarrow 0$) also varies with $P_{O_2}^{-1/4}$.

We conclude that the mechanisms of the electrode reaction for gauze and sputtered electrodes on Bi_2O_3-Er_2O_3 is the same whereas the actual contribution of the different processes is influenced by the morphology of the electrode.

Diffusion path.—The resistance R in the equivalent electrical circuit shown in Fig. 8a is connected with the electrolyte. The conclusion drawn in part I, that R is a diffusion resistance of atomic oxygen on the oxide surface, could not be explicitly proved by frequency dispersion. As discussed above the impedance of a diffusion process reduces to a resistive behavior for $\beta \leq 0.3$.

The Warburg impedance W cannot be correlated with diffusion of adsorbed oxygen atoms on the Pt surface because according to Eq. [7] we should have to find $K_w^{-1} \sim P_{O_2}^{1/2}$. Furthermore, if W is correlated with diffusion of oxygen atoms on the Pt surface the value of K_W should be independent of the electrolyte. However ,at 10^{-4} atm O_2 (973 K) K_W has a value of 2.4×10^{-3} Ωm^2 sec$^{-1/2}$ for BE20 and this is about 10 times lower than for ZY17 and CG10 (see Table II). We can conclude that the Warburg impedance W does not find its origin in diffusion of oxygen atoms on surfaces. The power 1/4 suggests that hole conduction plays a role. It may be that transport of holes from the electrode to electrolyte/gas interface is rate determining and that on this interface the charge transfer takes place,according to

$$O_{ads} \leftrightarrows O^{2-} + 2h^+ \qquad [11]$$

where h denotes a hole and $C_h \sim P_{O_2}^{1/4}$.

According to Eq. [7] and [8], $E_a(Z_W\ (\omega \rightarrow 0))$ are given by $E_a(C_h) + \frac{1}{2}\Delta H_{Dh}$ and $E_a(C_h) + \Delta H_{Dh}$, respectively, with $E_a(C_h)$ the formation enthalpy of free holes and ΔH_{Dh} the diffusion enthalpy for holes. From the experimental data for $E_a(K_W)$ and $E_a(Z_W\ (\omega \rightarrow 0))$ it follows that $E_a(C_h)$ is small and we find for ΔH_{Dh} a value of about 80 kJ mol^{-1}. This value is, however, lower than the activation energy measured for the hole conductivity of stabilized Bi_2O_3, which should have a value of 106 kJ mol^{-1} (24).

More study is necessary to elucidate the origin of Warburg impedance W. Up to this moment it is clear that W is typically for Bi_2O_3-based solid electrolytes and is not found for zirconia. In ceria-based electrolytes a Warburg component may play some role at high P_{O_2}.

Conclusions

1. The diffusion path which actually occurs in the electrode process on Pt/solid electrolyte combination is strongly influenced by the type of solid electrolyte.

2. For Pt electrodes on ZY17 frequency dispersion measurements showed that the rate-limiting steps are diffusion processes that are connected in series. At $P_{O_2} > P_{O_2}^{min.}$ ($\theta \approx 1$) diffusion of atomic oxygen at the anode (W_a) is rate determining and at $P_{O_2} < P_{O_2}^{min.}$ ($\theta << 1$) diffusion of atomic oxygen at the cathode (W_c) is rate determining. In part I it was concluded that these diffusion steps occur on the electrode surface. This study showed that diffusion on the electrolyte surface and through the electrolyte plays no significant role.

[2] Simulation shows that using a parallel combination of a $-1/2$ and $-1/4$ power yields a $-3/8$ power over 5 decades.

3. For Pt electrodes on CG10 frequency dispersion measurements showed that at $P_{O_2} < P_{O_2}^{min.}$ ($\theta << 1$) the electrode process is determined by diffusion at the cathode (W_c). This diffusion process shows the same characteristics as for Pt electrodes on ZY17. Therefore it was concluded that this diffusion process occurs on the electrode too. At $P_{O_2} > P_{O_2}^{min.}$ the electrode process is determined by a resistance, which is correlated with a charge transfer process (R_{ct}). Parallel to this resistance is a Warburg impedance, which is proposed to be correlated with the electrolyte: diffusion of oxygen atoms on the oxide surface or electronic conductivity through the electrolyte.

4. For Pt electrodes on BE20, BE30, and BE40 frequency dispersion measurements showed that two processes play a role, a resistance R and a Warburg impedance W which are connected parallel. From a comparison with other electrolyte-electrode combinations it is concluded that R is correlated with diffusion of atomic oxygen on the electrolyte surface at the cathode. The Warburg impedance is typically for Bi_2O_3-based materials and it is suggested that electronic charge carriers in the electrolyte are the diffusing species in this process.

At high P_{O_2} the d-c resistance of the electrode process is determined by the resistance R (diffusion on the electrolyte) and a low P_{O_2} by the Warburg impedance (diffusion through the electrolyte).

5. The magnitude of the double layer capacities C_{dl} are dependent on the nature of the solid electrolyte. For the Bi_2O_3-based materials they reach the very large value of about 15 **F**/m^2 for sputtered electrodes, whereas for substituted zirconia or ceria values of about 1-3 **F**/m^2 are found.

Acknowledgments

We would like to thank Mr. M. W. J. Hammink and Mr. J. M. Paauwe for experimental assistance and Dr. K. J. de Vries and Mr. H. Kruidhof for supplying the CeO_2-Gd_2O_3 sample. Prof. Dr. G. H. J. Broers is thanked for the stimulating discussions concerning Warburg impedance. Financial assistance from Philips N.V. (Elcoma) is gratefully acknowledged.

Manuscript submitted Jan. 27, 1982; revised manuscript received July 20, 1982.

Any discussion of this paper will appear in a Discussion Section to be published in the December 1983 JOURNAL. All discussions for the December 1983 Discussion Section should be submitted by Aug. 1, 1983.

Publication costs of this article were assisted by Twente University of Technology.

REFERENCES

1. M. J. Verkerk, M. W. J. Hammink, and A. J. Burggraaf, *This Journal*, **130**, 70 (1983).
2. J. E. Bauerle, *J. Phys. Chem. Solids*, **30**, 2657 (1969).
3. J. R. Macdonald, *J. Chem. Phys.*, **61**, 3977 (1974).
4. D. R. Franceschetti and J. R. Macdonald, *J. Electroanal. Chem. Interfacial Electrochem.*, **82**, 271 (1977).
5. E. Schouler, M. Kleitz, and C. Déportes, *J. Chim. Phys.*, **70**, 923 (1973).
6. E. Schouler, Ph.D. Thesis, Grenoble (1979).
7. S. H. Chu and M. A. Seitz, *J. Solid State Chem.*, **23**, 297 (1978).
8. S. P. S. Badwal and H. J. de Bruin, *Phys. Status Solidi A*, **49**, 261 (1979).
9. T. M. Gür, I. D. Raistrick, and R. A. Huggins, *Solid State Ionics*, **1**, 251 (1980).
10. H. Peters and K. H. Radeke, *Monats Ber. Det. Akad. Wiss. Berlin*, **10**, 819 (1968).
11. D. Braunshtein, D. S. Tannhauser, and I. Riess, *This Journal*, **128**, 82 (1981).
12. D. Y. Wang and A. S. Nowick, *ibid.*, **126**, 1166 (1979).
13. H. A. Harwig, Ph.D. Thesis, State University, Utrecht (1977).
14. H. T. Cahen, Ph.D. Thesis State University, Utrecht (1980).
15. G. H. J. Broers and M. Schenke, Proc. Int. Conf. on Fuel Cells, p. 299, Akademie Verlag, Dresden (1967).
16. T. M. Gür, Ph.D. Thesis, Stanford University (1978).
17. R. Lewis and R. Gomer, *Surf. Sci.*, **12**, 157 (1968).
18. M. Kleitz, Ph.D. Thesis, Grenoble (1968).
19. P. Fabry and M. Kleitz, *J. Electroanal. Chem. Interfacial Electrochem.*, **57**, 165 (1974).
20. J. Fouletier, P. Fabry, and M. Kleitz, *This Journal*, **123**, 204 (1976).
21. J. Fouletier, H. Seinera, and M. Kleitz, *J. Appl. Electrochem.*, **5**, 177 (1975).
22. I. V. Murygin and V. N. Chebotin, *Elektrokhimiya*, **15**, 1647 (1979).
23. G. H. J. Broers, Private communication.
24. T. Takahashi, T. Esaka, and H. Iwahara, *J. Appl. Electrochem.*, **7**, 303 (1977).
25. M. J. Verkerk, Ph.D. Thesis, Twente University of Technology, The Netherlands (1982).